Effects of Adhesive and Interphase Characteristics Between Matrix and Reinforced Nanoparticle of AA4032/ALN Nanocomposites

A. Chennakesava Reddy
Professor, Department of Mechanical Engineering,
JNTUH College of Engineering, Hyderabad, India

International Journal of Research in Mechanical Engineering
Volume 3, Issue 5, September-October, 2015, pp. 13-21
ISSN Online: 2347-5188 Print: 2347-8772, DOA: 14092015

ABSTRACT

Theoretical models were unable to examine the overall elastic-plastic response during the deformation of metal matrix composites. On the other hand, numerical micromechanical modeling analysis appears to be well-suited to describe the behavior of these composites. In this article two types of RVE models have been implemented using finite element analysis. Aluminum nitride nanoparticles were used as a reinforcing material in the matrix of AA4032 aluminum alloy. It has been observed that the nanoparticle did not overload during the transfer of load from the matrix to the nanoparticle via the interphase due to interphase between the nanoparticle and the matrix. Due to interphase between the nanoparticle and the matrix, the tensile strength increases from 510.60 to 532.51 MPa.

Keywords: *RVE Models, AlN, AA4032, Finite Element Analysis, Interphase.*

1. INTRODUCTION

Metal matrix composites (MMCs) have been drawn attention in recent years owing to the need for materials with high strength and stiffness in the field for a large number of functional and structural applications. The higher stiffness of ceramic particles can lead to an incremental increase in the stiffness of a composite [1, 2]. One of the major challenges when processing nanocomposites is achieving a homogeneous distribution of reinforcement in the matrix as it has a strong impact on the properties and the quality of the material. The current processing methods often generate agglomerated particles in the ductile matrix and as a result they exhibit extremely low ductility [3]. Particle clusters act as crack or decohesion nucleation sites at stresses lower than the matrix yield strength, causing the nanocomposite to fail at unpredictable low stress levels. Possible reasons resulting in particle clustering are chemical binding, surface energy reduction or particle segregation [4, 5, 6]. While manufacturing Al alloy-AlN nanocomposites, the wettability factor is the main concern irrespective of the manufacturing method. Its high surface activity restricts its incorporation in the metal matrix. One of the methods is to add surfactant which acts as a wetting agent in molten metal to enhance wettability of particulates. Researchers have successfully used several surfactants like Li, Mg, Ca, Zr, Ti, Cu, and Si for the synthesis of nanocomposites [7, 8, 9].

The objective of this article was to develop AA4032/AlN nanocomposites with and without wetting criteria of AlN by AA4032 molten metal. The RVE models were used to analyze the nanocomposites using finite Element analysis.

ISSN (O) 2347-5188
(P) 2347-8772

2. THEORETICAL BACKGROUND

Analyzing structures on a microstructural level, however, is clearly an inflexible problem. Analysis methods have therefore sought to approximate composite structural mechanics by analyzing a representative section of the composite microstructure, commonly called a Representative Volume Element (RVE). One of the first formal definitions of the RVE was given by Hill [10] who stated that the RVE was 1) structurally entirely typical of the composite material on average and 2) contained a sufficient number of inclusions such that the apparent moduli were independent of the RVE boundary displacements or tractions. Under axisymmetric as well as antisymmetric loading, a 2-D axisymmetric model can be applied for the cylindrical RVE, which can significantly reduce the computational work [11].

2.1 Determination of Effective Material Properties

To derive the formulae for deriving the equivalent material constants, a homogenized elasticity model of the square representative volume element (RVE) as shown in Fig.1 is considered. The dimensions of the three-dimensional RVE are $2a$ x $2a$ x $2a$. The cross-sectional area of the RVE is $2a$ x $2a$. The elasticity model is filled with a single, transversely isotropic material that has five independent material constants (elastic moduli E_y and E_z, Poison's ratios v_{xy}, v_{yz} and shear modulus G_{yz}). The general strain-stress relations relating the normal stresses and the normal stains are given below:

$$\varepsilon_x = \frac{\sigma_x}{E_x} - \frac{v_{xy}\,\sigma_y}{E_y} - \frac{v_{xz}\,\sigma_z}{E_z} \tag{1}$$

$$\varepsilon_y = -\frac{v_{yx}\,\sigma_x}{E_y} + \frac{\sigma_y}{E_y} - \frac{v_{yz}\,\sigma_z}{E_z} \tag{2}$$

$$\varepsilon_z = -\frac{v_{zx}\,\sigma_x}{E_x} - \frac{v_{zy}\,\sigma_y}{E_y} + \frac{\sigma_z}{E_z} \tag{3}$$

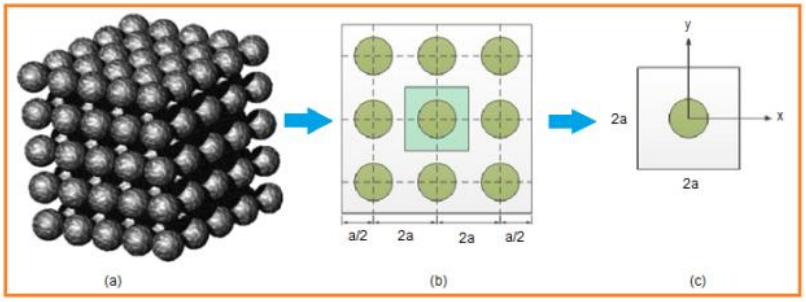

Fig.1 A Square RVE Containing a Nanoparticle

Let assume that $\sigma_{xy} = \sigma_{yx}, \sigma_{yz} = \sigma_{zy}$ and $\sigma_{zx} = \sigma_{xz}$. For plane strain conditions, $\epsilon_z = 0, \epsilon_{yz} = \varepsilon_{zx} = 0$ and $v_{yz} = v_{zx}$. The above equations are rewritten as follows:

$$\varepsilon_x = \frac{\sigma_x}{E_x} - \frac{v_{xy}\,\sigma_y}{E_y} - \frac{v_{yz}\,\sigma_z}{E_z} \tag{4}$$

$$\varepsilon_y = -\frac{v_{xy}\,\sigma_x}{E_y} + \frac{\sigma_y}{E_y} - \frac{v_{yz}\,\sigma_z}{E_z} \tag{5}$$

$$\varepsilon_z = -\frac{v_{yz}\,\sigma_x}{E_z} - \frac{v_{yz}\,\sigma_y}{E_z} + \frac{\sigma_z}{E_z} \tag{6}$$

ISSN (O) 2347-5188
(P) 2347-8772

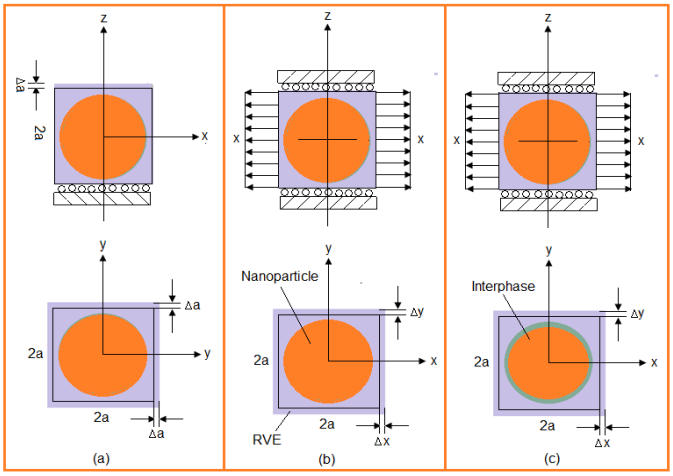

Fig. 2 RVE Models

To determine E_y and E_z, v_{xy} and v_{yz}, four equations are required. Two loading cases as shown in figure 2 have been designed to give four such equations based on the theory of elasticity. For load case (Fig.2a), the stress and strain components on the lateral surface are:

$$\sigma_x = \sigma_y = 0$$

$$\varepsilon_x = \frac{\Delta a}{a} \text{ along } x = \pm a \text{ and } \varepsilon_y = \frac{\Delta a}{a} \text{ along } y = \pm a$$

$$\varepsilon_z = \frac{\Delta a}{a}$$

where Δa is the change of dimension a of cross-section under the stretch Δa in the z-direction. Integrating and averaging Eq. (6) on the plane z = a, the following equation can be arrived:

$$E_z = \frac{\sigma_{ave}}{\varepsilon_z} = \frac{a}{\Delta a}\sigma_{ave} \quad (7)$$

where the average value of σz is given by:

$$\sigma_{ave} = \iint \sigma_z\,(x, y, a)dxdy \quad (8)$$

The value of σave is evaluated for the RVE using finite element analysis (FEA) results.

Using Eq. (5) and the result (7), the strain along $y = \pm a$:

$$\varepsilon_y = -\frac{v_{yz}\,\sigma_z}{E_z} = -v_{yz}\frac{\Delta a}{a} = \frac{\Delta a}{a}$$

Hence, the expression for the Poisson's ratio vyz is as follows:

$$v_{yz} = -1 \quad (9)$$

For load case (Fig. 2b), the square representative volume element (RVE) is loaded with a uniformly distributed load (negative pressure), P in a lateral direction, for instance, the x-direction. The RVE is constrained in the z-direction so that the plane strain condition is sustained to simulate the interactions of RVE with surrounding materials in the z-direction. Since $\varepsilon_z = 0$, $\sigma_z = v_{yz}(\sigma_x + \sigma_y)$ for the plain stress, the strain-stress relations can be reduced as follows:

$$\varepsilon_x = \left(\frac{1}{E_x} - \frac{1}{E_z}\right)\sigma_x - \left(\frac{v_{xy}}{E_y} + \frac{1}{E_z}\right)\sigma_y \quad (10)$$

$$\varepsilon_y = -\left(\frac{v_{xy}}{E_x} + \frac{1}{E_z}\right)\sigma_x + \left(\frac{1}{E_x} - \frac{1}{E_z}\right)\sigma_y \quad (11)$$

For the elasticity model as shown in figure 2b, one can have the following results for the normal stress and strain components at a point on the lateral surface:

 ISSN (O) 2347-5188
(P) 2347-8772

$\sigma_y = 0, \sigma_x = P$

$\varepsilon_x = \frac{\Delta x}{a}$ along $x = \pm a$ and $\varepsilon_y = \frac{\Delta y}{a}$ along $y = \pm a$

where Δx (>0) and Δy (<0) are the changes of dimensions in the x- and y- direction, respectively for the load case shown in figure 2b. Applying Eq. (11) for points along y = ±a and Eq. (10) for points along x = ±a, we get the following:

$$\varepsilon_y = -\left(\frac{v_{xy}}{E_x} + \frac{1}{E_z}\right)P = \frac{\Delta y}{a} \quad (12)$$

$$\varepsilon_x = \left(\frac{1}{E_x} - \frac{1}{E_z}\right)P = \frac{\Delta x}{a} \quad (13)$$

By solving Eqs. (12) and (13), the effective elastic modulus and Poisson's ratio in the transverse direction (xy-plane) as follows:

$$E_x = E_y = \frac{1}{\frac{\Delta x}{Pa} + \frac{1}{E_z}} \quad (14)$$

$$\mathrm{v_{xy}} = -\left(\frac{\Delta y}{Pa} + \frac{1}{E_z}\right)/\left(\frac{\Delta x}{Pa} + \frac{1}{E_z}\right) \quad (15)$$

In which E_z can be determined from Eq. (7). Once the change in lengths along x- and y- direction (Δx and Δy) are determined for the square RVE from the FEA, E_y (= E_x) and v_{xy} can be determined from Eqs. (14) and (15), correspondingly.

2.2 Empirical Models for Elastic Moduli and Strength of Nanocomposites

The strength of a particulate metal matrix composite depends on the strength of the weakest zone and metallurgical phenomena in it [12, 13]. A new criterion is suggested by the author considering adhesion, formation of precipitates, particle size, agglomeration, voids/porosity, obstacles to the dislocation, and the interfacial reaction of the particle/matrix. The formula for the strength of composite is stated below:

$$\sigma_c = \left[\sigma_m \left\{\frac{1-(v_p+v_v)^{2/3}}{1-1.5(v_p+v_v)}\right\}\right] e^{m_p(v_p+v_v)} + k d_p^{-1/2} \quad (16)$$

$$k = E_m m_m / E_p m_p$$

where, v_v and v_p are the volume fractions of voids/porosity and nanoparticles in the composite respectively, m_p and m_m are the possion's ratios of the nanoparticles and matrix respectively, d_p is the mean nanoparticle size (diameter) and E_m and E_p is elastic moduli of the matrix and the particle respectively. Elastic modulus (Young's modulus) is a measure of the stiffness of a material and is a quantity used to characterize materials. Elastic modulus is the same in all orientations for isotropic materials. Anisotropy can be seen in many composites. The proposed equations [12, 13] by the author to find Young's modulus of composites and interphase including the effect of voids/porosity as given below:

The upper-bound equation is given by

$$\frac{E_c}{E_m} = \left(\frac{1-v_v^{2/3}}{1-v_v^{2/3}+v_v}\right) + \frac{1+(\delta-1)v_p^{2/3}}{1+(\delta-1)(v_p^{2/3}-v_p)} \quad (17)$$

The lower-bound equation is given by

$$\frac{E_c}{E_m} = 1 + \frac{v_p - v_p}{\delta/(\delta-1)-(v_p+v_v)^{1/3}} \quad (18)$$

where, $\delta = E_p/E_m$.

ISSN (O) 2347-5188
(P) 2347-8772

The transverse modulus is given by

$$E_t = \frac{E_m E_p}{E_m + E_p(1-{v_p}^{2/3})/{v_p}^{2/3}} + E_m\left(1 - {v_p}^{2/3} - {v_v}^{2/3}\right) \quad (19)$$

The young's modulus of the interphase is obtained by the following formula:

$$E_i(r) = \left(\alpha E_p - E_m\right)\left(\frac{r_i - r}{r_i - r_p}\right) + E_m \quad (20)$$

3. MATERIALS METHODS

The matrix material was AA4032 aluminum alloy. AA4032 contains Si (12.50%), Cr (≤0.10%), Cu (1.20%), Fe (≤1.00%), Mg (1.10%), Ni (1.00%) and Zn (≤0.25%) as its major alloying elements. The reinforcement material was aluminum nitride (AlN) nanoparticles of average size 100nm. The mechanical properties of materials used in the present work are given in table 1.

Table 1: Mechanical Properties of AA4032 Matrix and ALN Nanoparticles

Property	AA4032	AlN
Density, g/cc	2.68	3.26
Elastic modulus, GPa	78.6	330
Ultimate tensile strength, MPa	379	270
Poisson's ratio	0.33	0.24

The representative volume element (RVE or the unit cell) is the smallest volume over which a measurement can be made that will yield a value representative of the whole. In this research, a cubical RVE was implemented to analyze the tensile behavior AA4032/AlN nanocomposites (figure 6). The determination of the RVE's dimensional conditions requires the establishment of a volumetric fraction of spherical nanoparticles in the composite. Hence, the weight fractions of the particles were converted to volume fractions. The volume fraction of a particle in the RVE ($V_{p,rve}$) is determined using Eq.(21):

$$v_{p,rve} = \frac{\text{Volume of nanoparticle}}{\text{Volume of RVE}} = \frac{16}{3} \times \left(\frac{r}{a}\right)^3 \quad (21)$$

where, r represents the particle radius and a indicates the diameter of the cylindrical RVE. The volume fraction of the particles in the composite (V_p) is obtained using equation

$$V_p = (w_p/\rho_p)/(w_p/\rho_p + w_m/\rho_m) \quad (22)$$

where ρ_m and ρ_p denote the matrix and particle densities, and w_m and w_p indicate the matrix and particle weight fractions, respectively.

The RVE dimension (a) was determined by equalizing Eqs. (21) and (22). Two RVE schemes namely: without interphase (adhesion) and with interphase were applied between the matrix and the filler. The loading on the RVE was defined as symmetric displacement, which provided equal displacements at both ends of the RVE. To obtain the nanocomposite modulus and yield strength, the force reaction was defined against displacement. The large strain PLANE183 element [14] was used in the matrix and the interphase regions in all the models. In order to model the adhesion between the interphase and the particle, a COMBIN14 spring-damper element was used. The stiffness of this element was taken as unity for perfect adhesion which could determine the interfacial strength for the interface region.

ISSN (O) 2347-5188
(P) 2347-8772

To converge an exact nonlinear solution, it is also important to set the strain rates of the FEM models based on the experimental tensile tests' setups. Hence, FEM models of different RVEs with various particle contents should have comparable error values. In this respect, the ratio of the tensile test speed to the gauge length of the specimens should be equal to the corresponding ratio in the RVE displacement model. Therefore, the rate of displacement in the RVEs was set to be 0.1 (1/min).

4. RESULTS AND DISCUSSION

The AlN/AA4032 nanocomposites with or without interphase were modeled using finite element analysis (ANSYS) to analyze the tensile behavior and fracture.

4.1 Tensile Behavior

An increase of AlN content in the matrix could increase the tensile strength of the nanocomposite (Fig. 3). The maximum difference between the FEA results without interphase and the experimental results was 54.20 MPa. This differentiation can be ascribed to lack of bonding between the AlN nanoparticle and the AA4032 matrix. The maximum difference between the FEA results with interphase and the experiments results was 68.00 MPa. This discrepancy can be credited to the presence of voids in the nanocomposites. The results obtained from author's model (with voids) were nearly equal to the experimental values with maximum variation of 26.49 MPa. On the other hand, the deviation of FEA (RVE model) results with the experimental results possibly was as a result of micro-metallurgical factors (such as formation of voids and nanoparticle clustering) that were not considered in the RVE models.

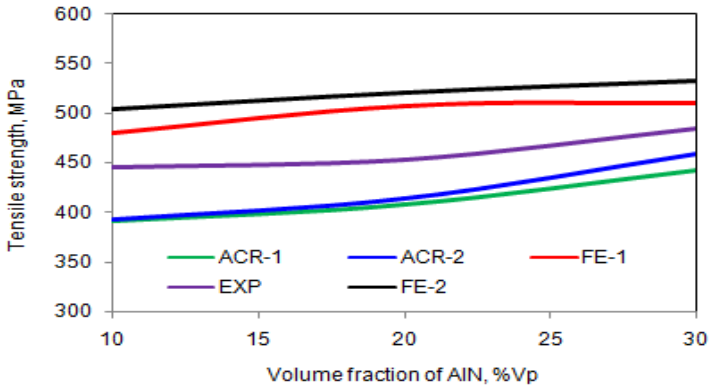

Fig. 3 Effect of Volume Fraction on Tensile Strength along Tensile Load Direction

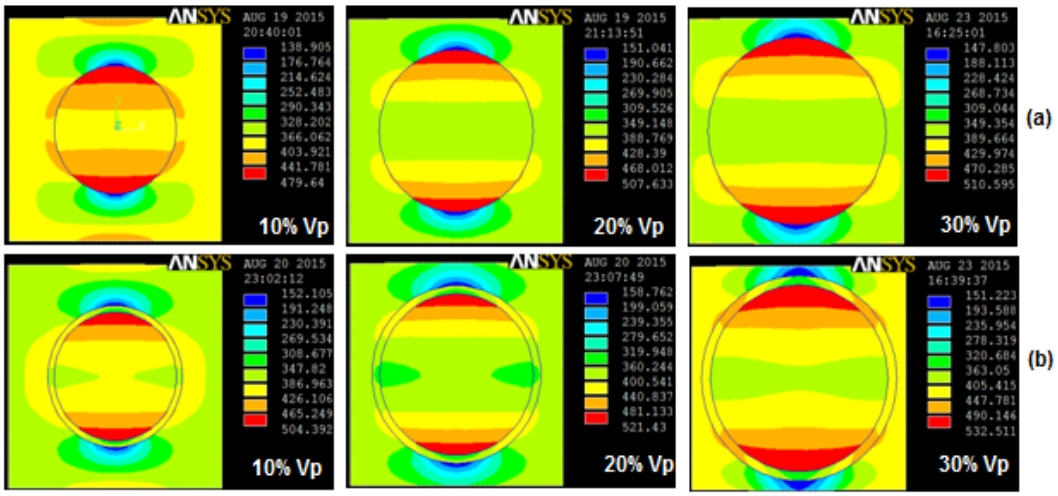

Fig.4 Tensile Stresses (A) Without Interphase and (B) With Interphase Normal to Load Direction

ISSN (O) 2347-5188
(P) 2347-8772

For 10%, 20% and 30%Vp of AlN in AA4032, without interphase and barely consideration of adhesive bonding between the AlN nanoparticle and the AA4032 matrix, the loads transferred from the AlN nanoparticle to the AA4032 matrix were, respectively, 75.72 MPa, 118.86 MPa and 120.95 MPa (Fig.4) along the tensile load direction. Similarly, for 10%, 20% and 30%Vp of AlN in AA4032, with interphase and wetting between the ALN nanoparticle and the AA4032 matrix, the loads transferred from the AlN nanoparticle to the AA4032 matrix were, respectively,117.43 MPa, 161.19 MPa and 169.46 MPa (figure 4) along the tensile load direction. Zhengang et al [15] carried a study improving wettability by adding Mg as the wetting agent. They suggested that the wettability between molten Al-Mg matrix and SiC particles is improved and the surface tension of molten Al-Mg alloy with SiC particle is reduced, and results in homogeneous particles distribution and high interfacial bond strength. For instance, addition of Mg to composite matrix lead to the formation of MgO and $MgAl_2O_3$ at the interface and this enhances the wettability and the strength of the composite [16].

According to strains developed in the nanocomposites (Fig.5), the RVE was expanded elastically away from the particle in the direction of the tensile loading. This would increase the contact area between the particle and the matrix in the perpendicular direction to the tensile loading and would decrease the contact area between the particle and the matrix in the direction of the tensile loading. The only difference is the amount of ductility achieved by the nature of bonding between the AlN nanoparticle and the AA4032 matrix. In another investigation [17] containing 15 vol% tetragonal DO_{23} structured $Al_3Zr_{25}Ti_{75}$, prepared by casting, was cold rolled to 0.017 per cent of the original thickness with a few intermediate anneals. While the intermetallic was fractured, the aluminum flow kept the interface intact and no cracks could be seen at aluminum intermetallic interfaces. The presence of interphase around the AlN nanoparticle has extended the yielding behavior.

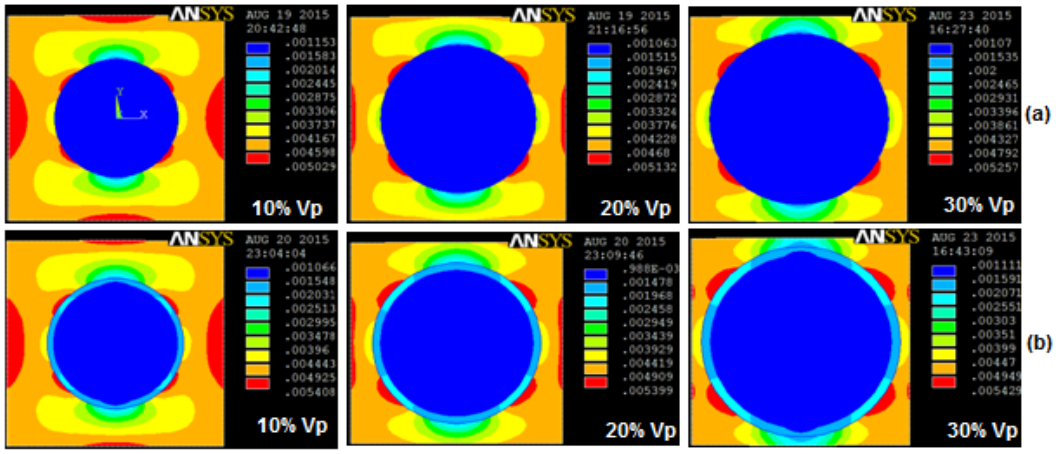

Fig.5 Elastic Strain (A) Without Interphase, Parallel, (B) With Interphase, Normal, (C) Without Interphase, Parallel And (D) With Interphase, Normal to Load Direction.

Table 2: Elastic Moduli of AA41032/Aln Nano Composite.

Source	Criteria	Longitudinal Elastic Modulus, GPa			Transverse Elastic Modulus, GPa		
		Vp = 10%	Vp = 20%	Vp = 30%	Vp = 10%	Vp = 20%	Vp = 30%
FEA	without interphase	95.45	98.92	97.13	95.57	99.05	97.26
FEA	with interphase	93.23	94.98	98.07	93.36	95.11	98.21
Author	upper limit	174.56	190.49	206.55	77.75	83.17	90.72
Author	lower limit	83.97	90.19	96.52	-	-	-
Rule of Mixture		103.74	128.88	154.02	85.08	92.73	101.89

ISSN (O) 2347-5188
(P) 2347-8772

The tensile elastic modulus increased appreciably with interphase around the AlN nanoparticle (table 2). It is observed that when the interphase is ignored the models with high filler contents give low values of elastic moduli. But it is known that the elastic moduli increase with filler content. Significant improvement in elastic moduli over the monolithic metal or alloy is achievable mainly because of excellent chemical bond between atoms of metal and the reinforcement.

4.2 Fracture

Fig. 6 depicts the increase of von Mises stress and shear stress with increase of volume fraction of AlN. In the case of nanocomposites with interphase between the nanoparticle and the matrix, the stress was transferred through shear from the matrix to the particles resulting low stress in the matrix. The stress transfer from the matrix to the nanoparticle was less for the nanocomposites without interphase resulting high stress in the matrix. Landis and McMeeking [17] assume that the fibers carry the entire axial load, and the matrix material only transmits shear between the fibers. Based on these assumptions alone, it is generally accepted that these methods will be most accurate when the fiber volume fraction V_f and the fiber-to matrix moduli *ratio* E_f / E_m are high. In the present case, the elastic moduli of AA4032 matrix and AlN nano particle are, respectively, 78.6 GPa and 330 GPa.

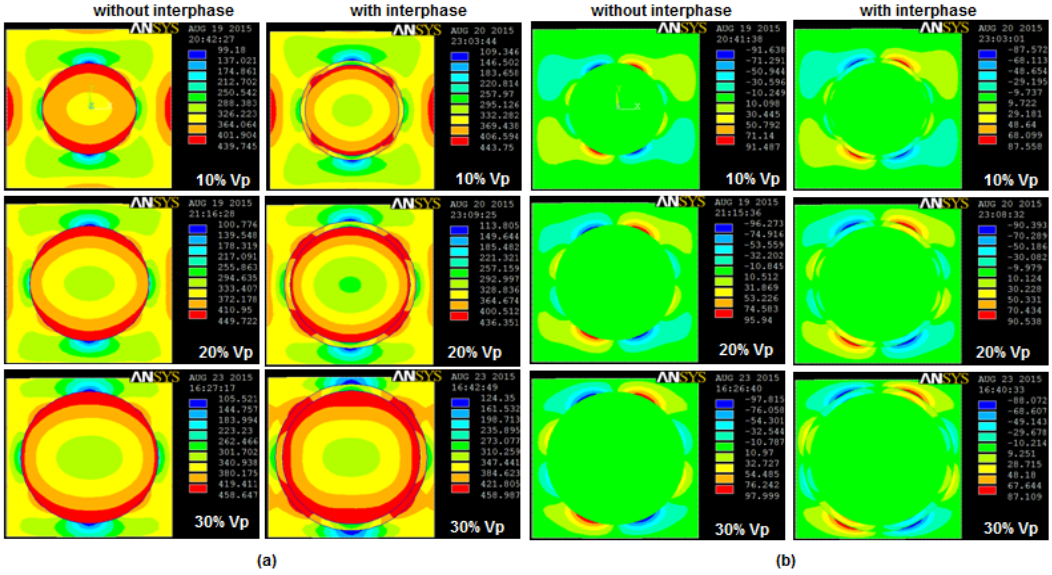

Fig.6 Von Mises Stress (A) and Shear Stress (B).

5. CONCLUSION

Without interphase and barely consideration of adhesive bonding, the tensile strength has been found to be 510.60 MPa for the nanocomposites consisting of 30%Aln nanoparticles. Due to interphase between the nanoparticle and the matrix, the tensile strength increases to 532.51 MPa. The tensile strengths obtained by author's model (with voids) are in good agreement with the experimental results. In the case of nanocomposites with interphase between the nanoparticle and the matrix, the stress is transferred through shear from the matrix to the particles. The transverse moduli of AlN/AA4032 nanocomposites have been found to be 97.26 GPa and 98.21 GPa, respectively, without and with interphase with 30 %Vp AlN nanoparticles in the composite.

REFERENCES

[1] A. Chennakesava Reddy, Mechanical Properties and Fracture Behavior of 6061/SiCp Metal Matrix Composites Fabricated by Low Pressure Die Casting Process, *Journal of Manufacturing Technology Research, 1(3/4)*, 2009, 273-286.

ISSN (O) 2347-5188
(P) 2347-8772

[2] A. Chennakesava Reddy and Essa Zitoun, Tensile Properties and Fracture Behavior of 6061/Al_2O_3 Metal Matrix Composites Fabricated by Low Pressure Die Casting Process, *International Journal of Materials Sciences, Vol. 6(2)*, 2011, 147-157.

[3] X. Deng and N. Chawla, Modeling the Effect of Particle Clustering on the Mechanical Behavior of SiC Particle Reinforced Al Matrix Composites, *Journal of Materials Science, 41*, 2006, 5731–5734.

[4] A.J. Reeves, H. Dunlop and T.W. Clyne, The effect of Interfacial Reaction Layer Thickness on Fracture of Titanium–SiC Particulate Composites, *Metallurgical Transactions A, 23*, 1992, 977–988.

[5] B. Kotiveerachari, A, Chennakesava Reddy, Interfacial Effect on the Fracture Mechanism in GFRP Composites, *CEMILAC Conf.*, Ministry of Defense, India, 1(b), 1999, 85-87.

[6] A. Chennakesava Reddy, Analysis of the Relationship between the Interface Structure and the Strength of Carbon-Aluminum Composites, *NATCON-ME*, Bangalore, 2004, 61-62.

[7] S. Ren, X. Shen, X. Qu and X. He, Effect of Mg and Si on Infiltration Behavior of Al alloys Pressureless Infiltration Into Porous SiCp Preforms, International Journal Minerals, *Metallurgy and Materials, 18 (6)*, 2011, 703–708.

[8] N. Sobczak, M. Ksiazek, W. Radziwill, J. Morgiel, W. Baliga and L. Stobierski, Effect of Titanium on Wettability and Interfaces in the Al/ SiC System, *in: Proc. of the International Conf. on High Temperature Capillarity*, Cracow, Poland, 1997.

[9] A.M. Davidson and D. Regener, A Comparison of Aluminum Based Metal Matrix Composites Reinforced with Coated and Uncoated Particulate Silicon Carbide, *Composites Science and Technology, 60(6)*, 2000, 865-869.

[10] R. Hill, Elastic Properties of Reinforced Solids: Some Theoretical Principles, *Journal of the Mechanics and Physics of Solids, 11*, 1963, 57-372.

[11] Y.J. Liu and X.L. Chen, Evaluations of the Effective Material Properties of Carbon Nanotube-Based Composites Using a Nanoscale Representative Volume Element, *Mechanics of Materials, 35*, 2003, 69–81.

[12] A. Chennakesava Reddy, Cause and Catastrophe of Strengthening Mechanisms in 6061/Al2O3 Composites Prepared by Stir Casting Process and Validation Using FEA, *International Journal of Science and Research, 4(2)*, 2015, 1272-1281.

[13] A. Chennakesava Reddy, Influence of Particle Size, Precipitates, Particle Cracking, Porosity and Clustering of Particles on Tensile Strength of 6061/SiCp Metal Matrix Composites and Validation Using FEA, *International Journal of Material Sciences and Manufacturing Engineering, 42(1)*, 2015, 1176-1186.

[14] Chennakesava R Alavala, *Finite Element Methods: Basic Concepts and Applications* (New Delhi, India: PHI Learning Pvt. Ltd, 2008).

[15] Zhengang Liuy, Guoyin Zu, Hongjie Luo, Yihan Liu and Guangchun Yao, Influence of Mg Addition on Graphite Particle Distribution in the Al Matrix Composites, *Journal of Materials Science & Technology, 26(3)*, 2010, 244-pp.244-250.

[16] A. Chennakesava Reddy and Essa Zitoun, Matrix Alloys for Alumina Particle Reinforced Metal Matrix Composites, *Indian Foundry Journal, 55(1)*, 2009, 12-16.

[17] P.A.Earvolino, M.E. Fine, J.R. Weertman and V.R. Parameswaran, Processing an Al/$Al_3Zr_{25}Ti_{75}$ Metal Matrix Composite by Conventional Melting, Casting & Rolling. *Scripta Metallurgica*, 26, 1992, 945-948.

[18] C.M. Landis and R.M. McMeeking, Stress Concentrations in Composites with Interface Sliding, Matrix Stiffness, and Uneven Fiber Spacing Using Shear Lag Theory, *International Journal of Solids Structures, 41*, 1999, 6289-6313.